ELSEVIER

Journal of Fluids and Structures 19 (2004) 93–110

JOURNAL OF FLUIDS AND STRUCTURES

www.elsevier.nl/locate/jnlabr/yjfls

Vibrations of plates with clamped and free edges excited by low-speed turbulent boundary layer flow

S.A. Hambric*, Y.F. Hwang, W.K. Bonness

Applied Research Laboratory, The Pennsylvania State University, P.O. Box 30, State College, PA 16804, USA

Received 21 June 2002; accepted 9 September 2003

Abstract

Plate vibrations due to turbulent boundary layer (TBL) excitation can depend strongly on the plate boundary conditions, especially when the flow convects over the plate at speeds much slower than those of the bending waves in the plate. The vibration response of a TBL excited baffled flat rectangular plate is analyzed with two sets of boundary conditions: (a) all four edges clamped, and (b) three edges clamped and one edge free, with the flow direction perpendicular to the free edge. A finite element model with discretization sufficient to resolve the convective wavenumbers in the flow excitation field is used for the study. Three TBL wall pressure excitation models are applied to the plates to represent the cross-spectra of the wall pressures: (i) a modified Corcos model, which includes all wavenumber components of excitation; (ii) a low-wavenumber excitation model previously derived by one of the authors, which only models the wavenumber-white region of the modified Corcos model; and (iii) an equivalent edge force model which only models the convective component in the modified Corcos model. The TBL wall pressure autospectrum is approximated using the model derived by Smolyakov and Tkachenko. The results obtained from applying models (ii) and (iii) to the clamped and free edge plates are compared to those generated using model (i). For the completely clamped boundary conditions, the low-wavenumber and Modified Corcos models yield nearly identical vibration spectra, indicating that surface interactions dominate the response of fully clamped plates excited by TBL pressures. For the free edge boundary condition, the vibrations predicted using the equivalent edge force and modified Corcos models match very well, showing that edge interactions between TBL pressures and structural modes dominate the vibrations of plates with free edges excited by TBL flow.

1. Introduction

Vibrations of thin-walled structures excited by high-speed turbulent flow, such as the baffled flat plate shown in Fig. 1, are caused by the wall pressure fields in the so-called 'convective ridge' region when flow speeds are equal to or higher than that of the structural wave speed. Fig. 2 compares a model of the wavenumber content of boundary layer wall pressures derived by Corcos (1963) and later modified by Hwang (1998) with the wavenumber transform of a flexural mode shape in a simply supported plate (the plot only shows wavenumber content in the flow, or streamwise direction). Fig. 2 corresponds to a case where the dominant modal wavenumber response ($k_m = m\pi/a$, where m is the mode order and a is the plate dimension) coincides with the dominant wavenumber range of the forcing function near the convective ridge, where $k = k_c = \omega/U_c$, or $kU_c/\omega = 1$, where ω is radial frequency and U_c is the convective flow speed. Strong structural acceptance of energy results in such a case. Fig. 3 shows a case where the wavenumber ratio between structural flexural response and wall pressures is quite low. Such conditions can be achieved by either stiffening

*Corresponding author. Tel.: +1-814-863-3030; fax: +1-814-863-1479.
E-mail address: sah@wt.arl.psu.edu (S.A. Hambric).

0889-9746/$ - see front matter
doi:10.1016/j.jfluidstructs.2003.09.002

Nomenclature

A_x, A_y	incremental plate areas
a	plate width
c_m	plate bending wavespeed at resonance frequency ω_m
D	plate flexural rigidity
f	cyclic frequency
$\boldsymbol{G}_{xx}$	cross-power spectral density matrix between inputs x
$\boldsymbol{G}_{yy}$	cross-power spectral density matrix between outputs y
$\boldsymbol{H}_{xy}$	transfer function matrix between inputs x and outputs y
J_1	Bessel function of the first kind
k	wavenumber
$\boldsymbol{k}$	wavevector
k_b	bending wavenumber
k_m	modal wavenumber
k_c	convective wavenumber
k_p	maximum wavenumber of integration
p	pressure
$R(\xi_1, \xi_3, \tau)$	space–time correlation of TBL wall pressure fluctuations
Re_δ	Reynolds number $= U_0\delta/v$
r	separation distance between points on plate surface
S_m	wavenumber sensitivity function
U_c	convective flow velocity
U_0	free stream velocity
x_μ, x_ν	excitation points on plate
y_i, y_j	response points on plate

Greek letters

α_1, α_3	decay constants for wall TBL pressure fluctuations in the streamwise (1) and cross-flow (3) directions
$\Gamma(\xi_1, \xi_3, \omega)$	coherence function of TBL wall pressure fluctuations
δ	boundary layer thickness
δ^*	boundary layer displacement thickness
η	structural loss factor
Λ_3	spanwise integral length scale of TBL wall pressure fluctuations
v	kinematic viscosity
ξ_1, ξ_3	separation distances
ρ	density
τ	time delay
τ_w	wall shear stress in boundary layer
$\hat{\Phi}_{pp}(\boldsymbol{k}, \omega)$	wavenumber–frequency spectrum of TBL wall pressure fluctuations
$\Phi_{pp}(x_\mu, x_\nu, \omega)$	cross-power spectral density function of TBL wall pressure fluctuations
$\Phi_{FF}(x_\mu, \omega)$	cross-power spectral density function of TBL wall force/length fluctuations along edge
$\phi_{pp}(\omega)$	autospectral density function of TBL wall pressure fluctuations
ω	radial frequency
ω_m	resonance frequency of mode m

the structure, thereby reducing its wavenumbers with respect to those in the wall pressures, or by slowing down the flow. In either case, the structure is excited mostly by the low-wavenumber content in the wall pressure field when k_m/k_c is small.

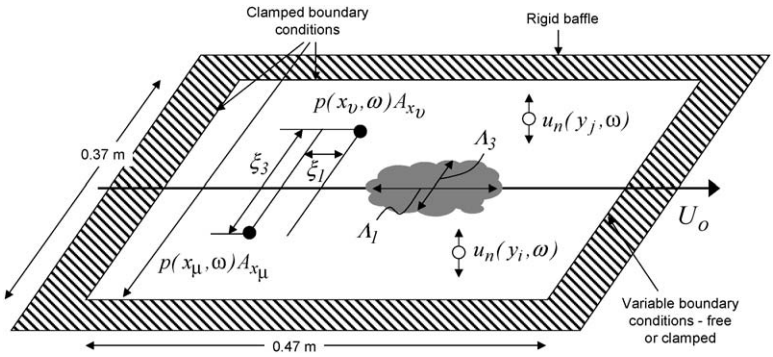

Fig. 1. TBL-excited baffled flat plate, pressures applied at points x_μ and x_v, normal velocity response at points y_i and y_j.

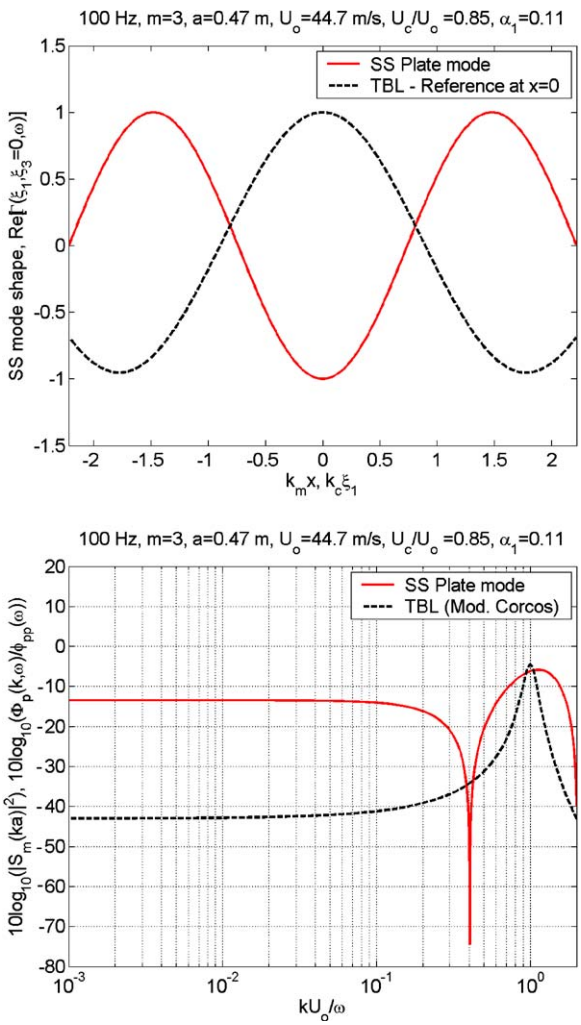

Fig. 2. TBL interaction with slow mode: top—$m = 3$ simply supported mode shape and real part of streamwise coherence function of TBL excitation (reference location at plate center); bottom—wavenumber transform of mode shape and coherence function.

The flexural vibration response of structures excited by slow moving turbulent boundary layers may be split into two regions (Chandiramani, 1977): the low-wavenumber region ($kU_c/\omega < 0.1$), where so-called 'surface interaction' dominates the structural acceptance of energy from the flow field, and the convective wavenumber region ($kU_c/\omega \sim 1.0$),

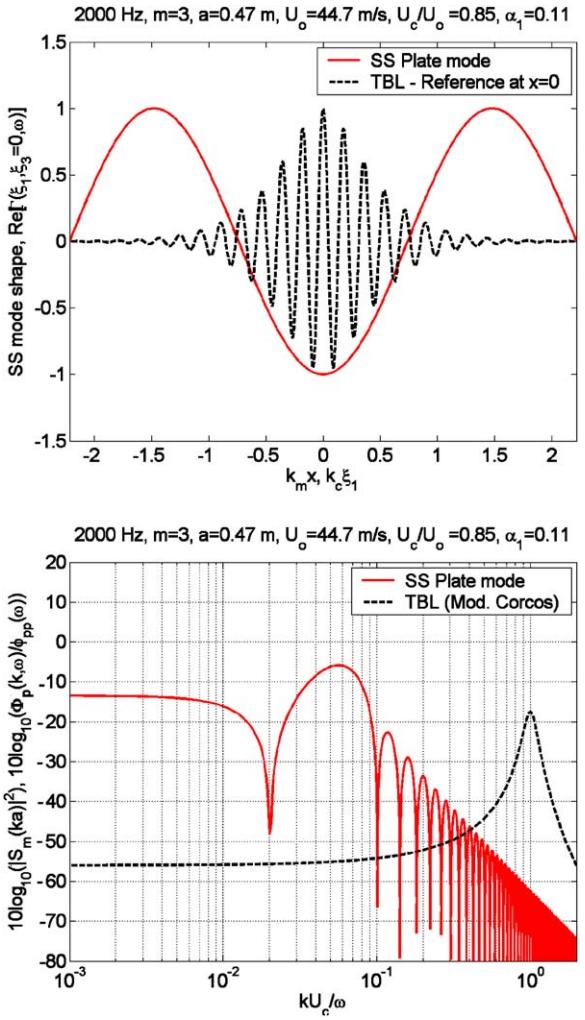

Fig. 3. TBL interaction with fast mode: top—$m = 3$ simply supported mode shape and real part of streamwise coherence function of TBL excitation (reference location at plate center); bottom—wavenumber transform of mode shape and coherence function.

where so-called 'edge interactions' dominate the response. Chandiramani postulated that the more discontinuous the response at an edge, the stronger the structural acceptance of energy, suggesting that structural regions with strong near-field behavior, such as those near free edges, will be well excited at convective wavenumbers.

In situations like those in Fig. 3, the plate flexural response is very sensitive to its boundary conditions (Hwang and Maidanik, 1990). Using analyses of the wall pressures and plate response in wavenumber space, Hwang and Maidanik found that the response of plates with clamped and simply supported edges excited by slow moving TBL flow was due almost entirely to acceptance of wall pressure energy in the low-wavenumber region, or surface interaction. When a plate edge is left free, however, the side lobes of the modal response function are stronger, and accept significant energy from the convective region. Fig. 4 compares the wavenumber transforms of mode shapes in simply supported, clamped, and free beams to a wavenumber–frequency model of the wall pressures for low- speed TBL flow, where

$$|S_m(ka)|^2 = \frac{2(k_m a)^2[1-(-1)^m\cos(ka)]}{[(ka)^2-(k_m a)^2]^2} \tag{1}$$

for simply supported boundary conditions,

$$|S_m(ka)|^2 = \frac{4}{[1-(k_m a)^{-1}]}\left[\frac{(k_m a)^2}{(k_m a)^2+(ka)^2}\right]^2 \times \left[\frac{\sin[(k_m-k)a/2]}{(k_m-k)a}+\frac{\sin[(k_m+k)a/2]}{(k_m+k)a}\right]^2 \tag{2}$$

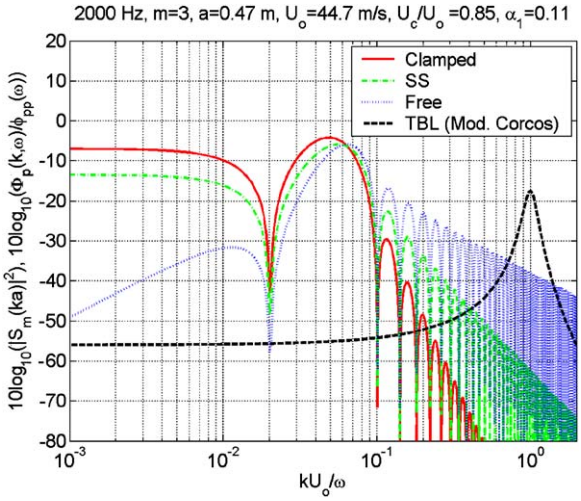

Fig. 4. Modal acceptance functions in wavenumber space for various boundary conditions along with real part of streamwise coherence function of TBL excitation.

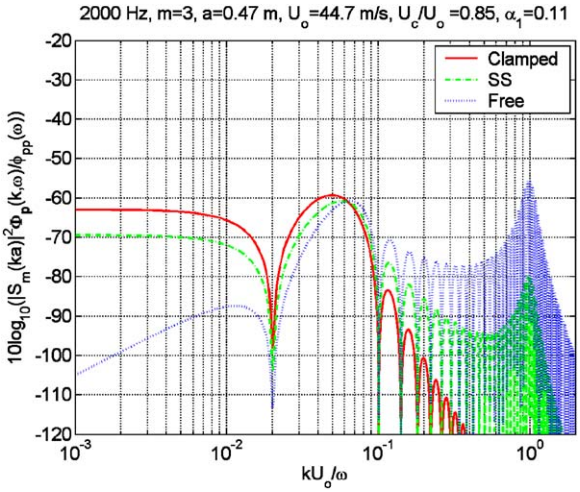

Fig. 5. Product of modal acceptance functions and TBL forcing functions for various boundary conditions.

for clamped boundary conditions, and

$$|S_m(ka)|^2 = \frac{2(ka)^2[1-(-1)^m\cos(ka)]}{[(ka)^2-(k_m a)^2]^2} \tag{3}$$

for free boundary conditions, where $|S_m(ka)|^2$ is a dimensionless wavenumber sensitivity function for each mode type, and where a is the beam length. (Note: the 'free' boundary condition case actually represents an edge condition where transverse motion is allowed, but rotational motion is restricted.) Fig. 5 compares the products of the modal acceptance functions with the TBL pressures. The free boundary conditions clearly increase the plate's acceptance of energy near the convective ridge and the simply supported and clamped boundary conditions result in very little excitation of the plate by convective ridge pressures.

Since most structures encountered in practice are not conducive to wavenumber analysis, computing the response of general systems to random inputs (such as TBL fluctuating wall pressures) must usually be conducted in physical space. An analysis approach in physical space, based on the methods of Bendat and Piersol (1986) and Lin (1967) for solving multiple-input -output problems, is discussed here. Finite element models are used to generate response functions and

empirical models are used to approximate the random forcing function under a turbulent boundary layer field. A validation exercise is conducted using measurements made at Purdue (Han et al., 1999).

The analysis approach will then be used to verify an approximate model proposed by Hwang (1998) that models only the low-wavenumber content, or surface interaction region, of the forcing function field. The low-wavenumber forcing function model, which reduces the required mesh density in the finite element model by ignoring the high-wavenumber forcing function content, should work very well when applied to plates with clamped boundary conditions based on the data shown in Figs. 4 and 5.

Since many practical structures excited by flow fields have free edges, the random analysis method is also used here to attempt to confirm Chandiramani's and Hwang and Maidanik's contention that analyzing the response of structures with free edges excited by boundary layer pressures requires including the energy in the convective wavenumbers in the analysis. To that end, an approximate forcing function model is investigated that considers edge interaction effects for TBL-excited plates with free edges.

Finally, infinite plate theory is used to generate mean-value response estimates that are compared to the finite plate vibration predictions. The accuracy of the mean-value response estimates for plates with clamped and free edges is discussed.

2. Analysis approach

Fig. 1 shows a baffled flat plate excited by TBL flow. Assuming the statistics of wall pressure fluctuations underneath turbulent boundary layers are stationary, the power spectral density of the resulting vibration between any two degrees of freedom (DOF) on the excited structure is

$$G_{uu}(y_i, y_j, \omega) = \int \int H^*_{u,F}(y_i/x_\mu, \omega)\Phi_{pp}(x_\mu, x_\upsilon, \omega)H_{u,F}(y_j/x_\upsilon, \omega)\,\mathrm{d}A_\mu\,\mathrm{d}A_\upsilon, \tag{4}$$

where G_{uu} is the displacement response cross-power spectral density between DOF y_i and y_j, $H_{u,F}(y_i/x_\mu, \omega)$ and $H_{u,F}(y_j/x_\upsilon, \omega)$ are frequency response functions relating displacements at response DOF y_i and y_j to forces applied at loaded points x_μ and x_υ (the asterisk denotes the complex conjugate), and $\Phi_{pp}(x_\mu, x_\upsilon, \omega)$ is the TBL pressure cross-power spectral density function applied to all loaded points. Note that the response DOF may be in any direction. In this paper, the response is taken to be normal to the plate surface. Also, pressure loads may theoretically be applied in any direction, but are assumed normal to the plate here.

The frequency response functions H may be generated from a variety of sources, such as analytical or finite element models, or from measured data. To accurately solve Eq. (4), both the spatial distributions of the response functions and forcing function must be adequately resolved. As we shall see, situations such as those depicted in Fig. 3 will require significant spatial resolution to resolve the small scales in the TBL wall forcing functions.

2.1. TBL wall pressure autospectrum and coherence models

Assuming a temporally stationary process, the cross-spectral density function $\Phi_{pp}(x_\mu, x_\upsilon, \omega)$ may be separated into an averaged autospectral density function $\bar{\phi}_{pp}(\omega)$ and a coherence function $\Gamma(\xi_1, \xi_3, \omega)$ between the loaded points x_μ and x_υ:

$$\Phi_{pp}(x_\mu, x_\upsilon, \omega) = \bar{\phi}_{pp}(\omega)\Gamma(\xi_1, \xi_3, \omega) \cong \sqrt{\phi_{pp}(x_\mu, \omega)\phi_{pp}(x_\upsilon, \omega)}\,\Gamma(\xi_1, \xi_3, \omega), \tag{5}$$

where $\bar{\phi}_{pp}(\omega)$ is approximated by the average of $\phi_{pp}(x_\mu, \omega)$ and $\phi_{pp}(x_\upsilon, \omega)$ and ξ_1 and ξ_3 are the streamwise and spanwise separation distances between points x_μ and x_υ.

Many investigators have proposed empirical models of $\phi_{pp}(\omega)$ and $\Gamma(\xi_1, \xi_3, \omega)$. See for example Bull (1996), Chase (1987) and Graham (1997). The autospectral density model proposed by Smolyakov and Tkachenko (1992) appears to work well in practice, and is used here to approximate $\phi_{pp}(\omega)$:

$$\phi_{pp}(\omega) \approx \left(\frac{\tau_w^2 \delta^*}{U_0}\right)\left(\frac{5.1}{1 + 0.44(\omega\delta^*/U_0)^{7/3}}\right), \tag{6}$$

where U_0 is the free-stream flow velocity, δ^* is the boundary layer displacement thickness, and τ_w is the wall shear stress which can be estimated for TBL flow with zero pressure gradient using the empirical relations $\mathrm{Re}_\delta \approx 8U_0\delta^*/\nu$ and $\tau_w \approx 0.0225\rho U_0^2/\mathrm{Re}_\delta^{0.25}$, where Re_δ is the boundary layer thickness Reynolds number, ν is the kinematic viscosity, and ρ is the fluid density.

Note that $\phi_{pp}(\omega)$ is a one-sided radial frequency spectrum, such that the mean square pressure fluctuation $\langle p^2 \rangle = \int_0^\infty \phi_{pp}(\omega)\,\mathrm{d}\omega$. To convert $\phi_{pp}(\omega)$ to a one-sided cyclic frequency spectral density $\phi_{pp}(f)$, Eq. (6) is multiplied by 2π.

$\Gamma(\xi_1, \xi_3, \omega)$ may be viewed as a coherence function of the fluctuating wall pressures, such that

$$\Gamma(\xi_1, \xi_3, \omega) = \frac{1}{2\pi} \int_{-\infty}^{\infty} R(\xi_1, \xi_3, \tau) \mathrm{e}^{-\mathrm{i}\omega\tau}\,\mathrm{d}\tau, \tag{7}$$

where R represents the space–time correlation of the fluctuating pressure field (assumed homogeneous) and Γ depends only on frequency and the separation vector (ξ_1, ξ_3) between points x_μ and x_υ in the plane of the flow. Several investigators have assumed that $\Gamma(\xi_1, \xi_3, \omega)$ may be separable in the streamwise and spanwise flow directions, including Corcos (1963), who proposed the well-known model:

$$\Gamma(\xi_1, \xi_3, \omega) = A(\omega\xi_1/U_c)B(\omega\xi_3/U_c), \tag{8}$$

where U_c is the average convection velocity of the flow, which is some fraction of the free stream velocity U_0. The convection velocity may be approximated (Bull, 1967) as a function of ω, U_0, and δ^* using the formula

$$U_c \cong U_0(0.59 + 0.30\mathrm{e}^{-0.89\omega\delta^*/U_0}). \tag{9}$$

Corcos postulated that the functions A and B may be represented as an exponentially decaying oscillating function in the flow direction and a simple exponentially decaying function in the cross-flow direction:

$$A(\omega\xi_1/U_c) = \mathrm{e}^{-\alpha_1|\omega\xi_1/U_c|}\mathrm{e}^{\mathrm{i}\omega\xi_1/U_c} \tag{10a}$$

and

$$B(\omega\xi_3/U_c) = \mathrm{e}^{-\alpha_3|\omega\xi_3/U_c|}, \tag{10b}$$

where α_1 and α_3 are decay constants in the streamwise and cross-flow directions, respectively.

Although Eq. (10) has been shown to work well for applications such as those depicted in Fig. 2, where the convective ridge region dominates the excitation of the structures, Eq. (10) overestimates the contributions of the low-wavenumber region of the TBL wall pressures. A modification to Eq. (10) has been proposed (Ko and Schloemer, 1989; Hwang, 1998) which distributes more of the TBL wall pressure energy near the convective ridge, thereby reducing the energy in the low-wavenumber region (since the mean square pressure must remain constant). The modification changes the function A to

$$A(\omega\xi_1/U_c) = (1 + \alpha_1|\omega\xi_1/U_c|)\mathrm{e}^{-\alpha_1|\omega\xi_1/U_c|}\mathrm{e}^{\mathrm{i}\omega\xi_1/U_c}. \tag{11}$$

2.2. Finite element analysis approach

The double integral in Eq. (4) may be solved using discretized numerical models, such as those generated using finite element (FE) analyses. The response cross-power spectral density is approximated by a double summation over all loaded points

$$G_{uu}(y_i, y_j, \omega) \cong \sum_{\mu=1}^{N} \sum_{\upsilon=1}^{N} H^*_{u,F}(y_i/x_\mu, \omega) A_{x_\mu} \Phi_{pp}(x_\mu, x_\upsilon, \omega) A_{x_\upsilon} H_{u,F}(y_j/x_\upsilon, \omega), \tag{12}$$

where A_{x_μ} and A_{x_υ} are the incremental surface areas of the loaded points.

Eq. (12) may be written in matrix form at a given frequency using the conventions of Bendat and Piersol (1986) and Lin (1967) as

$$\boldsymbol{G}_{yy} = \boldsymbol{H}^{*T}_{xy} \boldsymbol{G}_{xx} \boldsymbol{H}_{xy}, \tag{13}$$

where $\boldsymbol{G}_{yy}$ is a matrix of output cross-power spectral densities, $\boldsymbol{G}_{xx}$ is a matrix of input cross-power spectral densities, $\boldsymbol{H}_{xy}$ is a matrix of transfer functions relating response at the outputs to excitation at the inputs, x denote inputs and y denote outputs. The superscript T indicates a matrix transpose. The diagonal entries in the matrices $\boldsymbol{G}_{xx}$ and $\boldsymbol{G}_{yy}$ are auto-power spectral densities, and the off-diagonal entries represent cross-power spectral densities. An example of

Eq. (13) for two outputs and N inputs is

$$\boldsymbol{G}_{yy} = \begin{bmatrix} G_{y_1y_1} & G_{y_1y_2} \\ G_{y_2y_1} & G_{y_2y_2} \end{bmatrix} = \begin{bmatrix} H^*_{x_1y_1} & H^*_{x_2y_1} & \cdots & H^*_{x_Ny_1} \\ H^*_{x_1y_2} & H^*_{x_2y_2} & \cdots & H^*_{x_Ny_2} \end{bmatrix} \begin{bmatrix} G_{x_1x_1} & G_{x_1x_2} & \cdots & G_{x_1x_N} \\ G_{x_2x_1} & G_{x_2x_2} & \cdots & G_{x_2x_N} \\ \vdots & \vdots & & \vdots \\ G_{x_Nx_1} & G_{xNx_2} & \cdots & G_{x_Nx_N} \end{bmatrix} \times \begin{bmatrix} H_{x_1y_1} & H_{x_1y_2} \\ H_{x_2y_1} & H_{x_2y_2} \\ \vdots & \vdots \\ H_{x_Ny_1} & H_{x_Ny_2} \end{bmatrix}. \tag{14}$$

Note that the output points do not have to coincide with the input points. For example, the response of an object inside a flow-excited exterior surface may be solved for using Eq. (14).

A FE model is used to generate the entries of the $\boldsymbol{H}_{xy}$ matrix (response/force) and the approximate TBL forcing function models discussed earlier are used to generate the entries of the $\boldsymbol{G}_{xx}$ matrix, where

$$G_{x_\mu x_\upsilon}(\omega) = A_{x_\mu}\sqrt{\phi_{pp}(x_\mu,\omega)\phi_{pp}(x_\upsilon,\omega)}A_{x_\upsilon}\Gamma(\xi_1,\xi_3,\omega), \tag{15}$$

and $\phi_{pp}(\omega)$ is given by Eq. (6) and $\Gamma(\xi_1,\xi_3,\omega)$ is given by Eqs. (8), (10b), and (11).

Note that it is possible to estimate the total net force applied by the TBL pressure field to a structure by setting all transfer function values H to unity in Eq. (12).

2.3. Practical considerations and approximate TBL forcing function models

An example of the streamwise component of the modified Corcos model is shown in Fig. 6, along with two proposed approximate models for low-wavenumber surface forces and high-wavenumber edge forces. The TBL forcing function may be viewed as a combination of low-wavenumber (surface interaction), high wavenumber (edge interaction), and intermediate wavenumber contributions. For fixed boundary conditions, like simple or clamped supports, edge interaction is very low since plate motion is extremely small near the supports. Free edges, however, are free to move and will be well excited by edge forces.

In a TBL-excited FE model, many elements in the streamwise direction are typically required to resolve the convective part of the forcing function (the $e^{i\omega\xi_1/U_c}$ term in Eqs. (10a) and (11)). Since at low k_m/k_c (or U_c/c_m) ratios (less than about 0.1), where c_m is the plate bending wave speed at the resonance frequency ω_m of mode order m and $k_m = \omega_m/c_m$, plates with clamped and simply supported boundary conditions do not respond well to the convective forces (recall Figs. 3–5), so there is no need to include them in the model. A model including only the

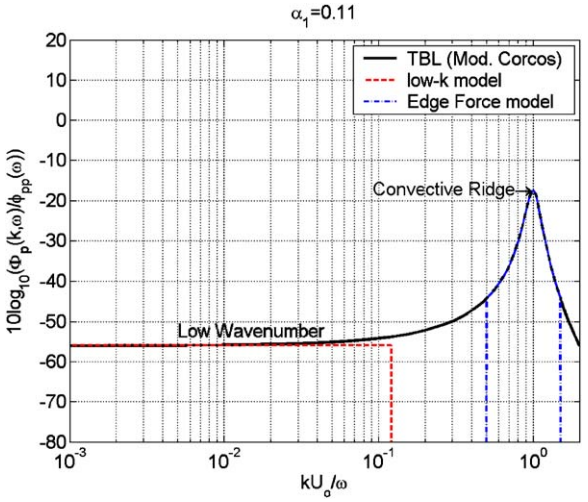

Fig. 6. Wavenumber regions where approximate surface (low-k) and edge force models apply.

wavenumber- white component (surface interaction) of the TBL wavenumber–frequency spectrum is given by

$$\frac{\hat{\Phi}_{pp}(\boldsymbol{k},\omega)}{\phi_{pp}(\omega)} = \hat{\Gamma}(\boldsymbol{k}\to 0,\omega) \cong \frac{1}{k_c^2}\frac{2\alpha_1^3}{\pi^2\alpha_3} \tag{16}$$

in wavenumber space. Using the transform definitions

$$\hat{\Gamma}(\boldsymbol{k},\omega) = \frac{1}{(2\pi)^2}\int_{-\infty}^{\infty}\int \Gamma(\boldsymbol{\xi},\omega)\mathrm{e}^{-\mathrm{i}\boldsymbol{k}\cdot\boldsymbol{\xi}}\,\mathrm{d}\xi_1\,\mathrm{d}\xi_3 \tag{17a}$$

and

$$\Gamma(\boldsymbol{\xi},\omega) = \int_{-\infty}^{\infty}\int \hat{\Gamma}(\boldsymbol{k},\omega)\mathrm{e}^{\mathrm{i}\boldsymbol{k}\cdot\boldsymbol{\xi}}\,\mathrm{d}k_1\,\mathrm{d}k_3 \tag{17b}$$

and by substituting Eq. (16) into Eq. (17b) and defining the vectors $\boldsymbol{k}$ and $\boldsymbol{\xi}$ as $(k_r\cos\theta, k_r\sin\theta)$ and (ξ_1,ξ_3) so that $\mathrm{e}^{\mathrm{i}\boldsymbol{k}\cdot\boldsymbol{\xi}} = \mathrm{e}^{\mathrm{i}\xi_1 k_r\cos\theta + \mathrm{i}\xi_3 k_r\sin\theta}$,

$$\Gamma(\boldsymbol{\xi},\omega) \cong \left(\frac{2\alpha_1^3}{\pi^2\alpha_3}\right)\left(\frac{1}{k_c}\right)^2\int_0^{k_p}\int_0^{2\pi}\mathrm{e}^{\mathrm{i}\xi_1 k_r\cos\theta+\mathrm{i}\xi_3 k_r\sin\theta}k_r\,\mathrm{d}\theta\,\mathrm{d}k_r, \tag{18}$$

where k_p is the maximum wavenumber of the integration.

By letting $r = \sqrt{\xi_1^2+\xi_3^2}$ and employing the definition $\mathrm{J}_0(k_r r) = \frac{1}{2\pi}\int_0^{2\pi}\mathrm{e}^{\mathrm{i}\xi_1 k_r\cos\theta+\mathrm{i}\xi_3 k_r\sin\theta}\,\mathrm{d}\theta$ (Courant and Hilbert, 1966), where J_0 is the 0th order Bessel function:

$$\Gamma(\boldsymbol{\xi},\omega) \cong \left(\frac{2\alpha_1^3}{\pi^2\alpha_3}\right)\left(\frac{1}{k_c}\right)^2 2\pi\int_0^{k_p}\mathrm{J}_0(k_r r)k_r\,\mathrm{d}k_r. \tag{19}$$

The integral in Eq. (19) may be evaluated using the definition (Wylie, 1960) $\int x\mathrm{J}_0(x)\,\mathrm{d}x = x\mathrm{J}_1(x)+C$, where x is $k_r r$ and $\mathrm{d}x$ is $r\,\mathrm{d}k_r$ here. The integral must be pre-multiplied by r^2/r^2 to be evaluated, which leads to

$$\frac{1}{r^2}\int_0^{k_p}\mathrm{J}_0(k_r r)rk_r r\,\mathrm{d}k_r = \frac{k_r r}{r^2}\mathrm{J}_1(k_r r)\Big|_0^{k_p} = k_p\frac{\mathrm{J}_1(k_p r)}{r}. \tag{20}$$

Multiplying the result by k_p/k_p and replacing r with $|\boldsymbol{\xi}|$ leads to the final definition for the low-wavenumber forcing function in physical space, where

$$\Gamma(\boldsymbol{\xi},\omega) \cong \left(\frac{2\alpha_1^3}{\pi^2\alpha_3}\right)\left(\frac{k_p}{k_c}\right)^2\left(2\pi\frac{\mathrm{J}_1(k_p|\boldsymbol{\xi}|)}{k_p|\boldsymbol{\xi}|}\right), \tag{21}$$

so that

$$\Phi_{pp}(\boldsymbol{\xi},\omega) \cong \left(\frac{2\alpha_1^3}{\pi^2\alpha_3}\right)\left(\frac{k_p}{k_c}\right)^2\bar{\phi}_{pp}(\omega)\left(2\pi\frac{\mathrm{J}_1(k_p|\boldsymbol{\xi}|)}{k_p|\boldsymbol{\xi}|}\right), \tag{22}$$

in which $\boldsymbol{\xi}$ is the vector between points x_μ and x_υ, k_p is the maximum wavenumber of excitation (typically set so as to span the major lobe of the modal sensitivity function, usually at least twice k_m, but not so high as to require unnecessarily fine discretization in the finite element mesh), k_c is the convective wavenumber, and J_1 is the Bessel function of the first kind.

Since plates with free edges respond very well to the convective portion of the TBL wavenumber–frequency spectrum (recall Fig. 5), even at low U_c/c_m ratios, the forcing functions may sometimes be approximated with edge interaction terms only. The edge force depends on the pressure levels and spatial coherence near the convective ridge ($U_c/c_m \sim 1$) and the shape of the excited mode at the plate edge. The force/length spectrum acting on a free edge normal to the flow (either upstream or downstream of the flow) may be approximated using methods from Hwang and Maidanik (1990) as

$$\Phi_{F'F'}(x_\mu,\omega) \cong \frac{\pi}{2}\left(\frac{1}{k_c}\right)^2\bar{\phi}_{pp}(\omega)\mathrm{e}^{-\alpha_3|\omega\xi_3/U_c|_\mu}, \tag{23}$$

where F' indicates force/length and the μ subscript on the argument of the exponential indicates that the function is evaluated at the reference location x_μ. A physical interpretation of Eq. (23) is to view the TBL loading as dominated by a strip of partially coherent forces acting along the free edge. To compute the resulting velocity spectra on the plate, the edge force/length spectrum must be integrated over the span of the excited edge:

$$G_{uu}(y_i,y_j,\omega) = \int\int H_{u,F}^*(y_i/x_\mu,\omega)\Phi_{F'F'}(x_\mu,\omega)H_{u,F}(y_j/x_\upsilon,\omega)\,\mathrm{d}L_\mu\,\mathrm{d}L_\upsilon. \tag{24}$$

Assuming the integration over the spanwise coherence portion of Eq. (23) returns the spanwise integral length scale Λ_{3_μ} (which is simply $U_c/(\alpha_3\omega)$ at location x_μ), and considering only the autospectrum at response point y_i, the integration may be approximated using a summation over the loaded points

$$G_{uu}(y_i, y_i, \omega) \cong \sum_{\mu=1}^{N} |H_{u,F}(y_i/x_\mu, \omega)|^2 \Phi_{F'F'}(x_\mu, \omega)\, \mathrm{d}L_{x_\mu} \Lambda_{3_\mu}. \tag{25}$$

By setting the H transfer functions equal to unity, the summation returns the total net applied edge force spectrum

$$\Phi_{FF}(\omega) \cong \frac{\pi}{2}\left(\frac{1}{k_c}\right)^2 \bar{\phi}_{pp}(\omega) \Lambda_3 L_3 \tag{26}$$

assuming Λ_3 is constant over the driven edge. The above approximations are valid for edges normal to a TBL flow field, either upstream or downstream of the flow. The approximate effects of TBL excitation on free edges tangent to the flow (pointing in the streamwise direction) are expected to be quite different, and are not addressed in this paper.

Both the low wavenumber and edge forcing function models do not require excessive discretization of FE models to be used accurately. FE meshes excited with the low-wavenumber forcing function model in Eq. (22) need only resolve the oscillations in the Bessel function with argument $k_p|\boldsymbol{\xi}|$. FE meshes excited with the approximate edge force/length model in Eq. (23) need only resolve the decay in the spanwise coherence component of Eq. (10b). FE meshes excited by either forcing function model must also represent adequately the mode shapes of interest, of course.

3. Numerical examples

FE models and measurements of a plate analyzed at Purdue University are used to verify the analysis approach and check the validity of the empirical TBL forcing function models. Next, a thickened version of Purdue's plate is used in a series of analytic/FE studies to investigate the validity and usefulness of the proposed approximate forcing function models for analyzing the vibrations of TBL-excited plates with clamped and free edges.

3.1. Verification of analysis approach—Purdue University flow excited plate

Measurements of vibration autospectra on a TBL-excited steel flat rectangular plate were made at Purdue University (Han et al., 1999) and are compared to predictions made using the approach discussed here. The plate is 47 cm long in the flow direction, 37 cm wide, and 0.159 cm thick and has a structural loss factor (where structural loss factor is defined as twice the damping ratio, where damping ratio is the damping coefficient divided by the critical damping coefficient) of about 0.005. The plate was flush mounted into the floor of a wind tunnel with screws to simulate clamped boundary conditions along the edges. The flow speed was 44.7 m/s (100 mph), and δ^* was measured to be 2.4 cm. Plate velocity autospectra were measured using a Scanning Laser Doppler Vibrometer (SLDV). Since the TBL behavior did not vary significantly over the plate, the wall pressure field was assumed to be spatially homogeneous, with constant values of α_1 and α_3 of 0.11 and 0.70.

In modelling the plate, enough elements were used to resolve both the structural modes and the convective term in the forcing function. Since the flow speeds are slower than the bending wavespeeds in the plate, the convective wavelength (U_c/f) dictates the element size required in the streamwise direction. At an analysis frequency of 600 Hz (the maximum frequency considered) and an approximate convection speed of 38 m/s, the minimum convective wavelength is about 6 cm. Therefore, to maintain at least eight elements over a convective wavelength, 60 elements were used in the flow direction.

Measured and predicted normal velocity autospectra at a point 15 cm from the plate's left edge and 12 cm from its bottom edge are shown in Fig. 7 and agree very well at frequencies above 150 Hz. The data does show that the two lowest plate resonances do not vibrate quite as strongly in the experiment as they do in the FE model. This may be due to slight differences between the actual and FE mode shapes (perhaps caused by the screws along the edge not simulating exactly clamped boundary conditions), or perhaps by inhomogeneities in the TBL field at low frequencies. In spite of the discrepancies at low frequencies, the majority of the data verifies the modelling approach, the TBL autospectrum model, and the Modified Corcos coherence model.

The wavenumber sensitivities of the plate investigated by Purdue are not in the low-wavenumber region of the forcing field, but are actually in an intermediate region ($U_c/c_m = k_m/k_c \sim 0.3$–$0.8$) where the wavenumber–frequency spectrum is increasing between the low-wavenumber white region and the convective ridge region. Therefore, to illustrate the accuracy of the approximate low-wavenumber (surface interaction) forcing function model, the plate is stiffened by

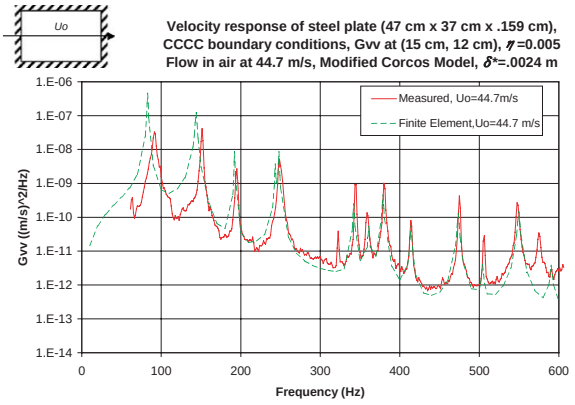

Fig. 7. Predicted and measured velocity spectra for Purdue plate at flow speed of 44.7 m/s. Thickened plate for approximate forcing function investigations.

increasing its thickness by a factor of ten (to 1.59 cm) to drive its modal wavenumber sensitivities into the low-wavenumber range of the TBL pressure forcing function (this is done by the increase in bending wavespeed c_B due to the thickness increase). The conditions shown in Figs. 4 and 5 correspond to an $m = 3$ mode in the stiffened plate near its resonance frequency of 2000 Hz, and clearly show that the clamped boundary condition case should accept very little energy from the convective ridge region of the TBL wall pressures.

The flow-excited thickened plate vibrations are analyzed for two boundary conditions, three flow speeds, and three structural loss factors (no attempt is made to include the effects of radiation damping or aerodynamic damping, which can be important for flow over free edges, in the predictions). The first boundary condition clamps the plate along all edges, and is denoted the 'CCCC' case. The second frees the edge perpendicular to and downstream of the flow. Free stream velocities of 44.7 m/s (100 mph), 89.4 m/s (200 mph) and 178.8 m/s (400 mph) were analyzed, along with structural loss factors of 0.005, 0.05, and 0.5 to examine the effects of varying loss factor and U_c/c_m (or k_m/k_c) on the accuracy of the approximate forcing function models. The point response 15 cm from the left edge and 12 cm from the bottom edge of the plate is computed and compared for the various conditions.

The mesh discretization in the streamwise direction was increased from the Purdue case, since stiffening the plate required increasing the maximum analysis frequency so that at least three to five resonance frequencies were spanned. The new maximum analysis frequency is 2000 Hz, and required 120 elements in the streamwise direction, corresponding to a minimum of five elements/wavelength. More elements would have been preferred, but the analysis times for such models would have been longer than desired. Some aliasing of the convective terms in the forcing function may occur at high frequencies and low speeds when exercising the full forcing function model, which points out the need for accurate, approximate forcing function models that do not require such dense FE meshes.

3.2. Clamped boundary conditions on all edges (CCCC case)

Fig. 8 shows sample predicted point vibration autospectra for a structural loss factor of 0.05 and the three flow speeds. Predictions made using the Modified Corcos and low-wavenumber forcing models are compared and show good agreement over most frequencies. At low frequencies and high flow speeds, the low-wavenumber forcing function model tends to underpredict the vibration levels, as it also does at high frequencies and low flow speeds. Fig. 9 compares vibration autospectra predictions at a flow speed of 89.4 m/s and three structural loss factors. The low-wavenumber forcing functions perform very well at all loss factors at this speed. Both figures show a discrepancy between the vibrations predicted using the Modified Corcos and low-wavenumber forcing models at frequencies below the first resonance. The discrepancy increases with increasing flow speed and decreasing frequency, and is due to the convective ridge contribution to the forces, which is neglected in the low-wavenumber forcing model.

Figs. 10 and 11 compare the predicted vibration levels at the resonance frequencies of the first and third modes of the plate as a function of flow speed and structural loss factor. The ratio of the convective velocity and the plate bending wave speed (U_c/c_m) are denoted for each flow speed in the plots. Recall that conditions similar to those depicted in Fig. 2 correspond to a U_c/c_m ratio of about 1, and conditions such as those shown in Fig. 3 correspond to a U_c/c_m ratio of less than 0.1.

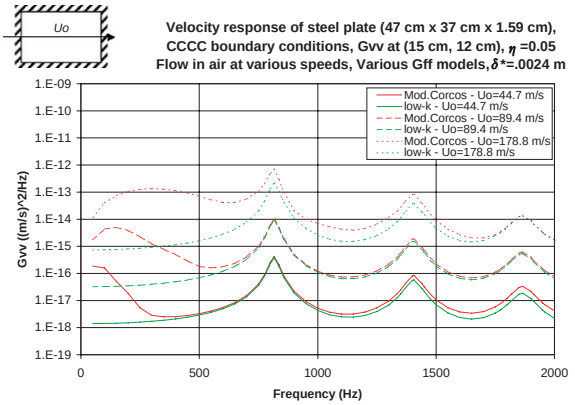

Fig. 8. Response of CCCC plate to Modified Corcos and approximate low-wavenumber (low-k) TBL forcing functions, structural loss factor = 0.05, variable flow speeds.

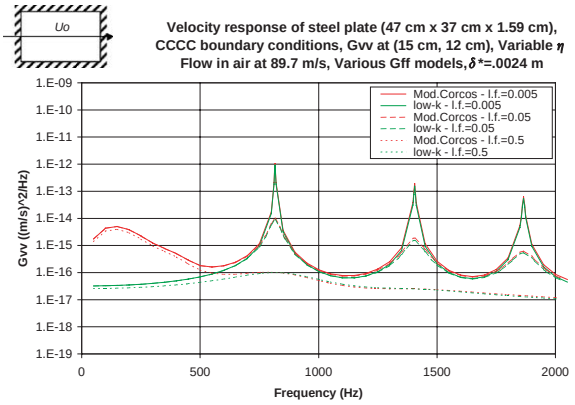

Fig. 9. Response of CCCC plate to Modified Corcos and approximate low-wavenumber (low-k) TBL forcing functions, flow speed of 89.7 m/s, variable loss factors.

For the first mode, the predicted vibration levels using both models agree very well at low flow speeds, but start to diverge at higher flow speeds where U_c/c_m starts to approach 1. This is expected since the low-wavenumber forcing function model is wavenumber white, and does not model the convective ridge region of the actual forcing function, nor the gradual increase in level between the low and convective wavenumber regions (the intermediate wavenumber region). For the third mode, the predicted vibration levels agree well except at low wavespeed ratios. The discrepancies at low U_c/c_m ratios are almost certainly due to slight aliasing of the convective part of the Modified Corcos model due to coarse discretization of the FE mesh at high frequencies and low flow speeds. The aliasing will artificially increase the levels predicted using the Modified Corcos model.

3.3. Clamped boundary conditions on three edges, free boundary conditions on one edge (CCFC case)

Fig. 12 shows sample predicted point vibration autospectra for a structural loss factor of 0.05 and the three flow speeds. Predictions made using the Modified Corcos and approximate edge forcing models are compared and show good agreement over most frequencies. At frequencies below the first plate resonance, the approximate edge force model underpredicts the vibration levels. The underpredictions worsen with increasing flow speed and decreasing frequency—conditions which lead to large surface integral length scales. These conditions invalidate the assumptions made when deriving the approximate edge force model, causing the approximate model to break down. At high frequencies and low flow speeds, the approximate edge forcing function model tends to underpredict the vibration levels. Fig. 13 compares vibration autospectra predictions made at a flow speed of 89.7 m/s and varying loss factors. As

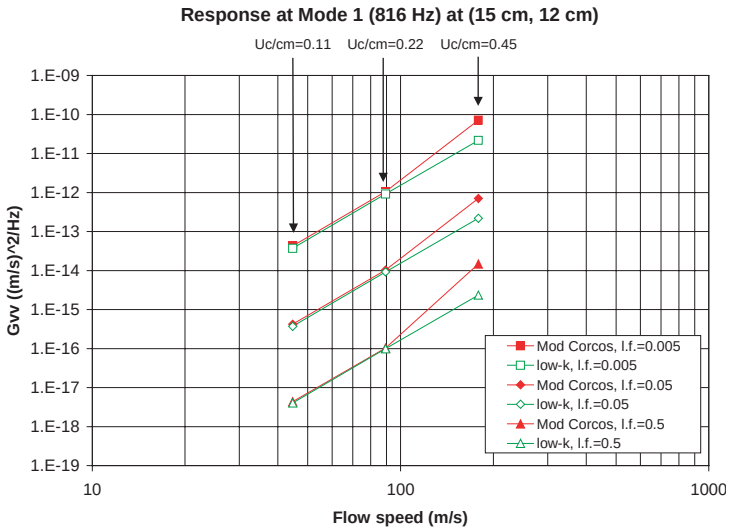

Fig. 10. Response of first mode of CCCC plate to Modified Corcos and low-wavenumber (low-k) TBL forcing functions.

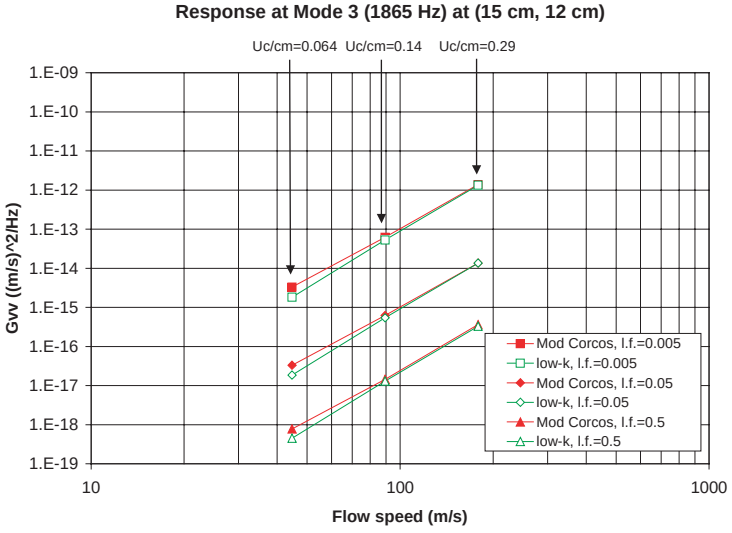

Fig. 11. Response of third mode of CCCC plate to Modified Corcos and low-wavenumber (low-k) TBL forcing functions.

in Fig. 12, the edge forcing function tends to cause an underprediction in vibration levels that worsens with increasing frequency.

Figs. 14 and 15 compare the predicted vibration levels at the resonance frequencies of the first and fifth modes of the plate as a function of flow speed and structural loss factor. The ratio of the convective velocity and the plate bending wave speed (U_c/c_m) are denoted for each flow speed in the plots. In contrast to the CCCC case, the approximate edge force model works best when U_c/c_m approaches 1, since the edge force approximates pressures near the convective ridge. When U_c/c_m decreases, surface interaction terms become more important, and the edge force underpredicts the vibration levels. Also, the underpredictions of the vibration levels using the approximate edge force model appear to worsen with increasing structural loss factor. This is likely due to the increased contributions from non-resonant modes to the vibration response, many of which are excited by the low-wavenumber region of the TBL flow, which is a surface interaction effect.

The accuracy of the approximate edge force/length spectrum may be further assessed by comparing the net edge force spectrum integrated over the free edge (Eq. (26)) to the net force estimated by integrating over the full Modified Corcos

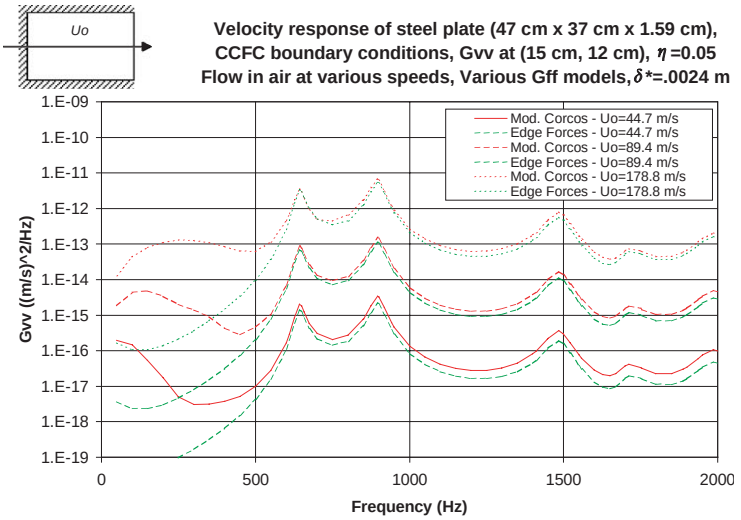

Fig. 12. Response of CCFC plate to Modified Corcos and approximate edge force TBL forcing functions, structural loss factor = 0.05, variable flow speeds.

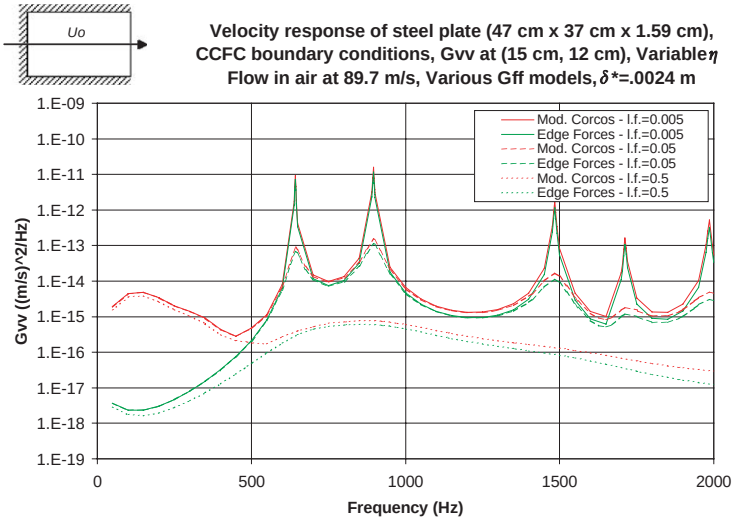

Fig. 13. Response of CCFC plate to Modified Corcos and approximate edge force TBL forcing functions, flow speed of 89.7 m/s, variable loss factors.

forcing function (result of Eq. (12) with transfer functions set to unity). The net force spectra for the full Modified Corcos and the approximate edge force models are compared in Fig. 16 for the three analysis speeds. Since the integration over the full model will return uncancelled forces over the edges both upstream and downstream of the flow, the approximate edge force model, applied only on the downstream, or free edge, must be doubled for the comparison. The integration of the full model shows some oscillations over frequency, especially at the highest speed, but the mean level matches the approximate edge force level very well. At high frequencies, the total force from the approximate edge force model is slightly lower than that of the full model, perhaps due to aliasing of the oscillations in the full model. The aliasing is more prevalent at lower speeds and higher frequencies, as discussed previously.

3.4. Approximation of mean value velocity spectra using infinite plate theory

In some cases, the mean values of the plate velocity autospectra may be approximated by using frequency response functions from infinite plate theory to populate the $\boldsymbol{H}_{xy}$ matrix used in the calculations. The admittance

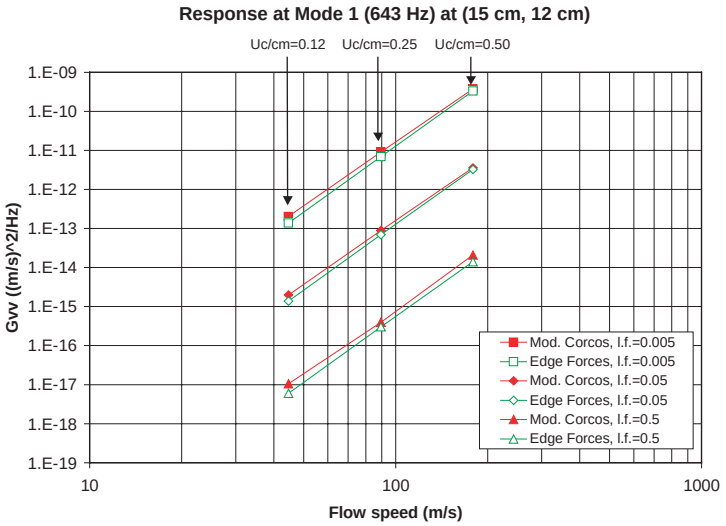

Fig. 14. Response of first mode of CCFC plate to Modified Corcos and edge force TBL forcing functions.

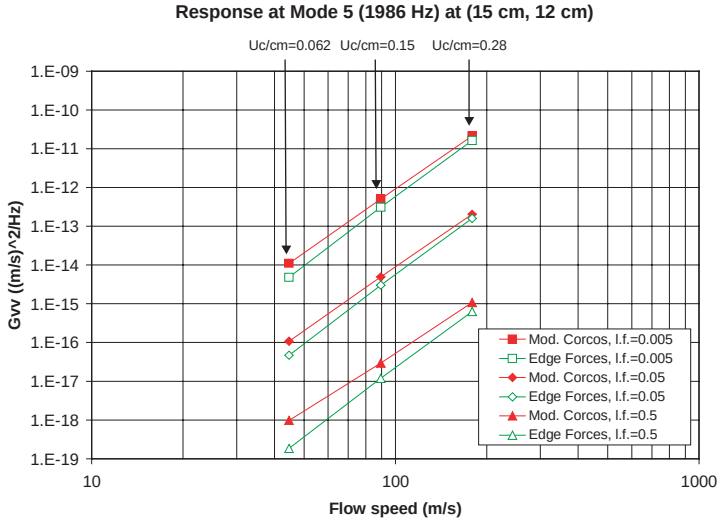

Fig. 15. Response of fifth mode of CCFC plate to Modified Corcos and edge force TBL forcing functions.

(velocity/pressure) of an infinite plate (in wavenumber space) is

$$\hat{H}_{u,p}(\boldsymbol{k},\omega)=\frac{-\mathrm{i}\omega}{D(k^4-k_B^4(1+\mathrm{i}\eta))}, \tag{27}$$

where D is the plate flexural rigidity.

Comparing the plate admittance to the TBL forcing function at low U_c/c_m conditions shows that virtually no energy is accepted by the plate from the convective terms (see Fig. 17). The low-wavenumber–frequency limit of the TBL forcing function, $\Phi_{pp}(k\to 0,\omega)=(1/k_c)^2(2\alpha_1^3/(\pi^2\alpha_3))\phi_{pp}(\omega)$, may therefore be combined with Eq. (27) and integrated over wavenumber space to calculate the forced response

$$G_{uu}(\omega)_{\infty}=\frac{\pi^2\omega^2}{2D^2k_B^6\eta}\left(\frac{1}{k_c}\right)^2\frac{2\alpha_1^3}{\pi^2\alpha_3}\phi_{pp}(\omega). \tag{28}$$

Note that the response is predicted to decrease with increasing structural loss factor, since the peak in the infinite plate wavenumber sensitivity function decreases with increasing structural loss factor (see Fig. 17).

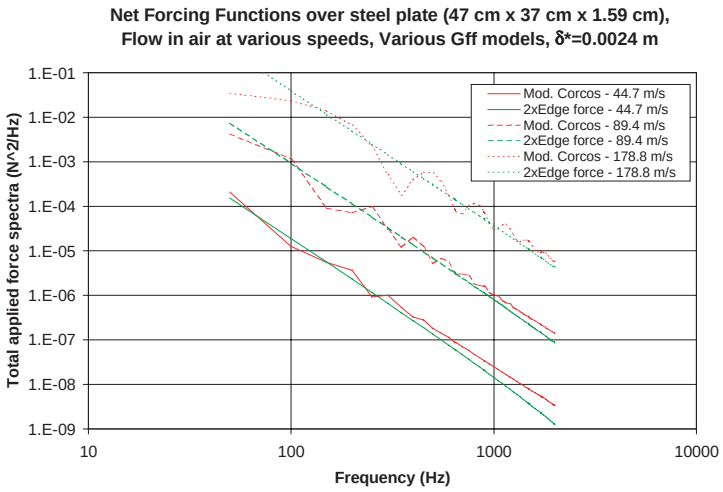

Fig. 16. Integrated net forcing functions applied by full (Modified Corcos) and approximate edge force models.

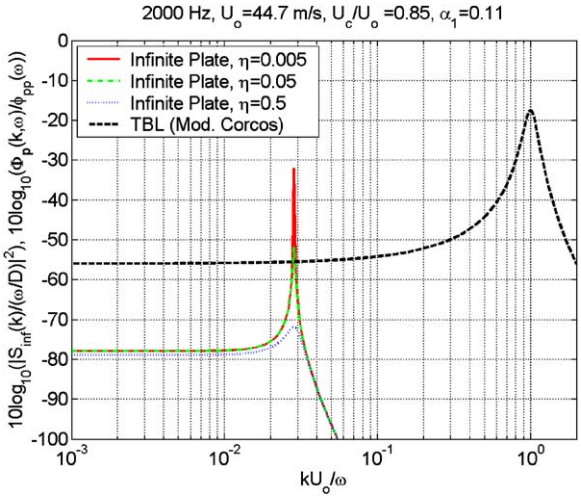

Fig. 17. Infinite plate response functions for variable loss factors compared to TBL wavenumber–frequency spectrum.

Predictions of the mean value response made using Eq. (28) are compared to predictions of the finite plate response in Fig. 18 for the CCCC case and Fig. 19 for the CCFC case for a speed of 89.4 m/s and varying loss factor. The infinite plate theory predicts the mean velocity response of the CCCC plate very well for all loss factors considered. The mean response of the CCFC plate, however, is generally higher than that predicted using infinite plate theory. Even for very high loss factors, the plate with the free edge still accepts significant energy from the convective terms in the TBL forcing function. Therefore, using Eq. (28) for predicting the mean response of plates with free edges is not recommended.

4. Summary and conclusions

Analyses of flow-excited vibrations of plates with clamped and free edges were conducted at low U_c/c_m (or k_m/k_c) ratios to examine the relative importance of surface and edge interaction between the plate structural modes and the TBL wall pressure wavenumber content. Also, approximate forcing function models that represent only the surface interaction, or low-wavenumber TBL forcing function content (for the fully clamped plate) and the edge interaction, or convective wavenumber TBL forcing function content (for the plate with a free edge) were evaluated using the analyses.

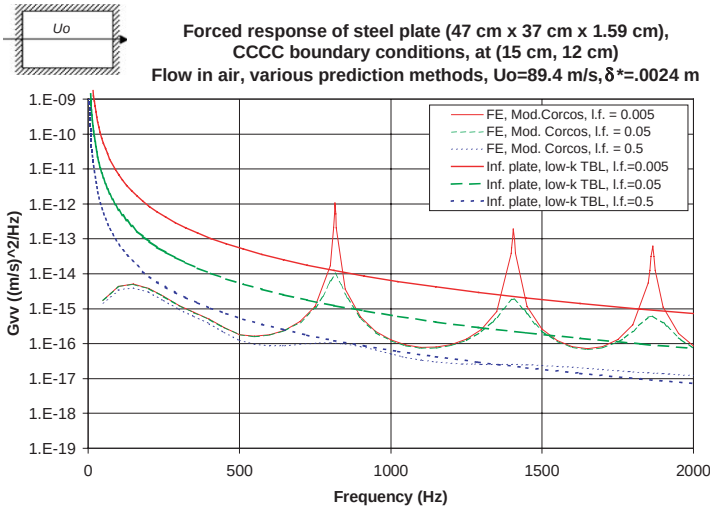

Fig. 18. Finite and infinite plate velocity response predictions for CCCC plate at 89.4 m/s, variable loss factors.

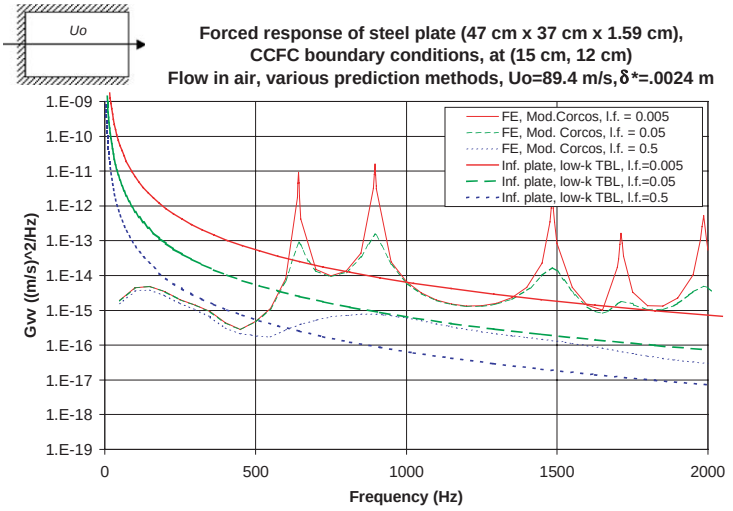

Fig. 19. Finite and infinite plate velocity response predictions for CCFC plate at 89.4 m/s, variable loss factors.

Hwang and Maidanik's (1990) assertion that free edged structures accept significant energy at convective wavenumbers even at low U_c/c_m ratios appears to be correct. Also, the approximate edge force spectrum presented appears to provide reasonable accuracy for U_c/c_m ratios > 0.1 for lightly damped structures. The approximate edge forcing function does not appear to work as well for heavily damped structures where non-resonant modes excited by surface interaction effects contribute more to the plate response.

Also as reported by Hwang and Maidanik (1990), clamped plates respond very little to edge forces, and are dominated by surface interaction (or low-wavenumber) forcing function content. The approximate low-wavenumber forcing function model therefore appears to work very well for plates with clamped boundary conditions and at low U_c/c_m (or k_m/k_c) ratios. The low-wavenumber forcing function model is not applicable, however, when U_c/c_m ratios approach 1. Structural loss factor does not appear to have a significant impact on the accuracy of the low-wavenumber forcing function model.

For fully clamped plates and U_c/c_m ratios much less than 1, infinite plate theory may be used to generate estimates of the mean velocity response of finite TBL excited plates. Such estimates should not be used, however, for plates with free edges.

The approximate models presented here, although proven useful, should be used with great care. U_c/c_m ratios at all resonances of interest, along with the structural loss factor (and radiation or aerodynamic loss factors, if they are significant) should be examined carefully to ensure the structural response will not be dominated by effects not modelled in the approximate forcing functions. In the future, approaches which retain the complete wavenumber content of the TBL forcing function but that are more computationally efficient should be investigated.

Acknowledgements

The authors acknowledge gratefully financial support from the Office of Naval Research (ONR) Code 334, Stephen Schreppler, contract monitor.

References

Bendat, J.S., Piersol, A.G., 1986. Random Data: Analysis and Measurement Procedures, 2nd Edition. Wiley, New York.

Bull, M.K., 1967. Wall pressure fluctuations associated with subsonic turbulent boundary layer flow. Journal of Fluid Mechanics 28, 719–754.

Bull, M.K., 1996. Wall-pressure fluctuations beneath turbulent boundary layers: some reflections on forty years of research. Journal of Sound and Vibration 190, 299–315.

Chandiramani, K.L., 1977. Vibration response of fluid-loaded structures to low-speed flow noise. Journal of the Acoustical Society of America 61, 1460–1470.

Chase, D.M., 1987. The character of the turbulent wall pressure spectrum at subconvective wavenumbers and a suggested comprehensive model. Journal of Sound and Vibration 112, 125–147.

Corcos, G.M., 1963. Resolution of pressure in turbulence. Journal of the Acoustical Society of America 35, 192–199.

Courant, R., Hilbert, D., 1966. Methods of Mathematical Physics, Vol. 1. Interscience, New York, p. 341.

Graham, W.R., 1997. A comparison of models for the wavenumber–frequency spectrum of turbulent boundary layer pressures. Journal of Sound and Vibration 206, 541–565.

Han, F., Bernhard, R.J., Mongeau, L.G., 1999. Prediction of flow-induced structural vibration and sound radiation using energy flow analysis. Journal of Sound and Vibration 227, 685–709.

Hwang, Y.F., 1998. A discrete model of turbulence loading function for computation of flow-induced vibration and noise. Proceedings of 1998 IMECE, Noise Control and Acoustics Division, Anaheim, CA, USA. pp. 389–395.

Hwang, Y.F., Maidanik, G., 1990. A wavenumber analysis of the coupling of a structural mode and flow turbulence. Journal of Sound and Vibration 142, 135–152.

Ko, S.H., Schloemer, H.H., 1989. Calculations of turbulent boundary layer pressure fluctuations transmitted into a viscoelastic layer. Journal of the Acoustical Society of America 85, 1469–1477.

Lin, Y.K., 1967. Probabilistic Theory of Structural Dynamics. McGraw-Hill, New York.

Smolyakov, A.V., Tkachenko, V.M., 1992. Model of a field of pseudosonic turbulent wall pressures and experimental data. Soviet Physics—Acoustics 37, 627–631.

Wylie, C.R., 1960. Advanced Engineering Mathematics, 2nd Edition. McGraw-Hill, New York, p. 427.